

Optical properties of $\text{Sr}_2\text{SiO}_4:\text{Eu}^{2+}$, Dy^{3+} phosphors prepared by combustion method

DURGA VERMA¹, R. P. PATEL^{2,*}, MOHAN L. VERMA¹

¹Department of Applied Physics, Faculty of Engineering and Technology, Shri Shankaracharya Group of Institutions, Shri Shankaracharya Technical Campus, Bhilai (C.G.) 490020, India

²Department of Applied Physics, Professional Institute of Engineering and Technology, Raipur (C.G.) 493225, India

In the present paper, TL and PL study of Dy^{3+} doped $\text{Sr}_2\text{SiO}_4:\text{Eu}^{2+}$ phosphor is reported. A polycrystalline sample of $\text{Sr}_2\text{SiO}_4:\text{Eu}^{2+}$, Dy^{3+} was prepared by combustion method. The obtained phosphor was characterized by powder X-ray diffraction, scanning electron microscopy, UV-Vis spectroscopy, PL and thermoluminescence. The results of the XRD studies obtained for $\text{Sr}_2\text{SiO}_4:\text{Eu}^{2+}$, Dy^{3+} phosphor revealed its monoclinic structure. The average crystallite size was calculated as 12.77 nm. Thermoluminescence study was carried out for the phosphor using UV irradiation and a single glow peak was found. The thermoluminescence glow curves of the samples were measured at various concentrations of co-dopant. The kinetic parameter has been calculated using Chen's glow curve method. In this paper, the photoluminescence and afterglow behavior of these phosphors are reported.

Keywords: *thermoluminescence; combustion method; XRD; photoluminescence*

1. Introduction

Materials that present long lasting phosphorescence (LLP) are potential candidates for the use in photonics applications, such as display technology and lighting [1], especially, since the discovery of $\text{Sr}_2\text{SiO}_4:\text{Eu}^{2+}$, Dy^{3+} in the middle of the 1990s [2]. Strontium orthosilicate exists in two crystallographic structures, viz. α' - Sr_2SiO_4 (orthorhombic) and β - Sr_2SiO_4 (monoclinic) [3]. The transition between the β -phase and the high temperature α' phase occurring at 385 K involves the rearrangement of SiO_4 tetrahedra without disconnection of the bonds [4, 5].

There are different types of scientific techniques for sample preparation, such as sol-gel [6, 7] co-precipitation and hydrothermal synthesis methods [8, 9] which have been adjusted to phosphors. All of these methods use liquid components that can be accurately controlled and thoroughly mixed. Combustion synthesis is a fast convenient reaction with increased efficiency.

The synthesis of phosphors by using the combustion method can produce a homogenous product in a short time without use of expensive high-temperature furnaces. This synthesis technique makes use of the heat energy liberated by the exothermic redox reaction between metal nitrates and urea or other fuels at a relatively low ignition temperature [10]. The particles of phosphors prepared using the conventional solid-state reaction are not suitable for the desired applications. The combustion method has been proven to be a facile route for the low-temperature preparation of various homogenous phosphors, including silicates and aluminates, in a short time [11–13].

Thermoluminescence (TL) is the phenomenon of light emission upon heating a material, which has been previously excited. All types of radiations, such as gamma rays, X-rays, alpha rays, beta rays and light rays can 'excite' a material, but to widely different extents. Out of the excitation energy imparted, a very large portion is almost instantaneously dissipated by various processes such as heat and light and only the rest is absorbed and stored. On subsequent heating, the energy may be

*E-mail: dbanchhor16@gmail.com

released and some of it may be in the form of light, which we call thermoluminescence [14, 15]. The important application fields of TL materials is TL dosimetry.

In this work, combustion synthesis was used to prepare $\text{Sr}_2\text{SiO}_4:\text{Eu}^{2+}$, Dy^{3+} phosphor using urea as a fuel and NH_4Cl as a flux. The properties of $\text{Sr}_2\text{SiO}_4:\text{Eu}^{2+}$, Dy^{3+} powders were characterized by powder X-ray diffraction (XRD), scanning electron microscopy (SEM), and UV-Vis spectroscopy. The studies of optical properties were also performed on the basis of thermoluminescence (TL) and photoluminescence (PL).

2. Experimental

$\text{Sr}_2\text{SiO}_4:\text{Eu}^{2+}$, Dy^{3+} phosphors were synthesized by combustion method. The raw materials: strontium nitrate $\text{Sr}(\text{NO}_3)_2$, 99.99 %, silica gel 99.99 %, europium oxide Eu_2O_3 , 99.99 % and dysprosium oxide Dy_2O_3 , 99.99 % were used as the starting materials. The starting materials were weighted according to the stoichiometry. In addition, Eu_2O_3 and Dy_2O_3 , taken as co-activators, were dissolved in concentrated nitric acid (HNO_3) before transferring them to the crucible. A small amount of ammonium chloride (NH_4Cl) was used as a flux, while the urea ($\text{CO}(\text{NH}_2)_2$) as a combustion fuel [16, 17]. The weighed quantities of each nitrate, flux and fuel were mixed in a mortar for 15 min to convert the constituents into a thick paste. The prepared paste was then placed in a vertical cylindrical muffle furnace maintained at 700 °C. Then, the prepared samples were annealed at 800 °C for 2 h under an air atmosphere.

The crystalline structure, size and phase composition of the samples were examined by PANalytical diffractometer using $\text{CuK}\alpha$ radiation ($\lambda = 1.5406 \text{ \AA}$), where X-ray was generated at 40 kV/30 mA voltage and current values, respectively. The scanning electron microscopy (ZEISS EVO 18) was used to observe particle morphology of the phosphors. Absorption spectra were recorded using (Shimadzu UV-1700 UV-Vis) spectrophotometer. Thermoluminescence was studied with PC based thermoluminescence

analyzer (10091). The samples were irradiated with UV-ray source. In photoluminescence spectra (PL), excitation and emission were recorded by spectrofluorometer (PerkinElmer LS45). All experiments were performed in identical conditions and it was observed that the results were reproducible.

3. Result and discussion

3.1. Optical band gap determining

The band gap is defined as the energy difference between the top of the valence band and the bottom of the conduction band. Electrons are generally able to jump from one band to another as long as a specific minimum amount of energy for the transition, i.e. the band gap energy, is provided. The optical band gap was calculated using absorption edge values (λ edge, in nm) from absorption spectra.

In Fig. 1a the absorption spectra of pure Sr_2SiO_4 and $\text{Sr}_2\text{SiO}_4:\text{Eu}^{2+}(0.1)$, $\text{Dy}^{3+}(0.2)$ are shown in the wavelength range of 200 nm to 500 nm. It can be seen that there is no absorption up to 250 nm and it increases at lower wavelength. The absorption edges found for pure Sr_2SiO_4 and $\text{Sr}_2\text{SiO}_4:\text{Eu}^{2+}$, Dy^{3+} are 225 nm and 230 nm, respectively.

The band gap energy can be determined using the Tauc relation [18–21]. It is a convenient way of studying the optical absorption spectrum of a material. Tauc equation 1 relates the absorption coefficient α and incident photon energy $h\nu$ by the following relation:

$$\alpha(h\nu) = \frac{B(h\nu - E_g)^n}{h\nu} \quad (1)$$

where E_g is the band gap, constant B is the correction coefficient, $h\nu$ is energy of photon, n is an index which assumes the values 1/2, 3/2, 2 and 3, depending on the nature of electronic transition responsible for the reflection. The value of the exponent n denotes the nature of the sample transition [18].

When $n = 2$, the equation 1 stands for the direct band gap and the band gap energy can be calculated by the equation:

$$E_g = \frac{hc}{\lambda} \quad (2)$$

where h is Planck constant, c is speed of light and λ is the related wavelength.

Fig. 1b shows a plot of $(\alpha h\nu)^2$ versus $(h\nu)$ according to the equation 1 and equation 2, where ν is the light frequency. The plot can be extrapolated by a straight line, giving the direct band gap value at the intercept with energy axis. The estimated values of optical direct band gap in the material are 5.52 eV and 5.4 eV for Sr₂SiO₄ and Sr₂SiO₄:Eu²⁺, Dy³⁺, respectively. The band gap of pure Sr₂SiO₄ material is of 0.12 eV wider compared to Sr₂SiO₄:Eu²⁺, Dy³⁺. This confirms that the carrier concentration in a doped material is increased compared to pure Sr₂SiO₄. The new electronic states created below the conduction band of the material may reduce the band gap of the Sr₂SiO₄:Eu²⁺, Dy³⁺. It was also explained by Vijayalakshmi et al. [22], who reported that in Zn doped SnO₂ the band gap value decreased. The optical band gap of Sr₂SiO₄:Eu²⁺, Dy³⁺ shifts towards the higher wavelength region (visible region) [23].

3.2. Structural analysis X-ray diffraction (XRD)

The analysis of XRD data of Sr₂SiO₄ phase is usually qualitative, just based on relative peak intensities. The typical X-ray diffraction patterns for combustion synthesized Sr₂SiO₄:Eu²⁺ phosphor powders in presence of different Dy³⁺ concentrations are shown in Fig. 2. It can be seen that the diffraction peaks of all the samples could be indexed to the monoclinic phase of β -Sr₂SiO₄ (Ref. code 98-003-5667). An estimation of average crystallite size for the sample is done using Scherer formula [24, 25]:

$$L = \frac{0.94\lambda}{\beta \cos \theta} \quad (3)$$

where L is the crystallite size, λ is the wavelength (for CuK α , $\lambda = 1.5406$ Å), β is the full width at

half maximum (FWHM) and θ is the Bragg's angle. Table 1 shows the calculation results of XRD data for Sr₂SiO₄:Eu²⁺, Dy³⁺ phosphor. The peaks in XRD patterns of different samples are similar to each other and are attributed to Sr₂SiO₄ monoclinic phase. The calculated average crystallite size of Sr₂SiO₄:Eu²⁺, Dy³⁺ phosphor is 12.77 nm.

Table 1. XRD data of Sr₂SiO₄:Eu²⁺, Dy³⁺ doped material.

2 θ	I/I ₀ [%]	FWHM [β]	Crystallite size [nm]	Lattice spacing [Å]	(h k l)
25.0260	20.37	0.7488	10.80	3.55531	(1 1 1)
27.4103	12.49	0.7488	10.91	3.25123	(1 1 3)
30.8088	34.68	0.7488	11.0	2.89989	(0 1 3)
31.3317	100	0.624	13.22	2.85268	(1 0 2)
31.6852	31.51	0.748	11.02	2.82166	(2 0 2)
31.9169	79.86	0.4056	20.36	2.80170	(1 1 3)
39.3022	16.64	0.6240	13.5	2.29057	(2 1 4)
44.0596	22.12	0.7488	11.4	2.05364	(2 2 0)

3.3. Morphological characterization: scanning electron microscopy (SEM)

The luminescence properties of phosphor particles depend on the morphology of the particles, such as size, shape, defects and so on. The morphology and topography of the samples were studied using scanning electron microscopy (SEM). The surface morphology of the Sr₂SiO₄:Eu²⁺, Dy³⁺ phosphor is shown in Fig. 3a and Fig. 3b at different magnifications. The surface morphology of the particles is not uniform and they form aggregates. The agglomerated particles, pores and voids are the result of gases released during the combustion process [26].

3.4. Thermoluminescence studies

Thermoluminescence is one of the possible ways to estimate the trap states of a material. Thermoluminescence (TL) consists in the light emission after removal of the source of exciting energy light, UV, gamma, X-rays, or other radiation; the free electrons may be trapped at an energy level higher than their ground state by application of thermal energy. The transition of electrons directly from

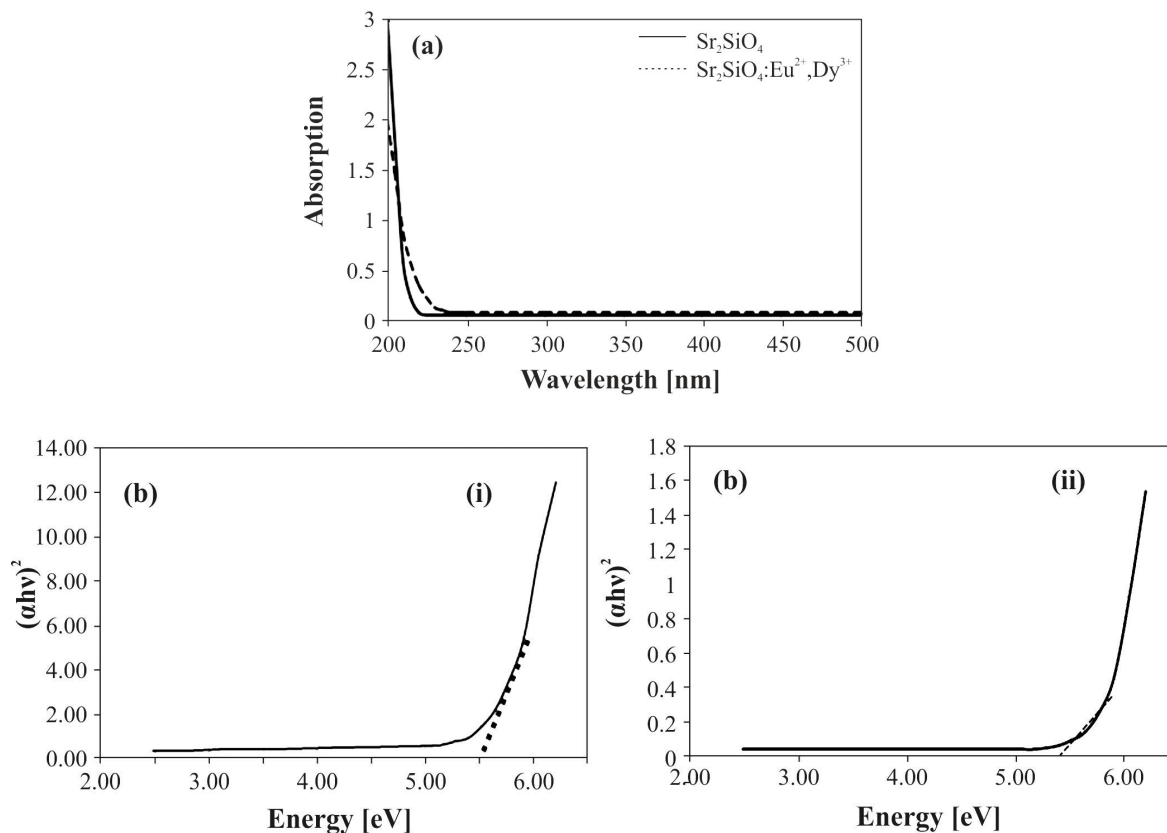


Fig. 1. (a) absorption spectra of pure Sr_2SiO_4 and $\text{Sr}_2\text{SiO}_4:\text{Eu}^{2+}, \text{Dy}^{3+}$ having absorption edges at 225 nm and 230 nm, (b) and (c) plots of $(\alpha h\nu)^2$ against energy E (eV) with band gap values for (i) $\text{Sr}_2\text{SiO}_4 = 5.52$ eV and (ii) $\text{Sr}_2\text{SiO}_4:\text{Eu}^{2+}, \text{Dy}^{3+} = 5.4$ eV.

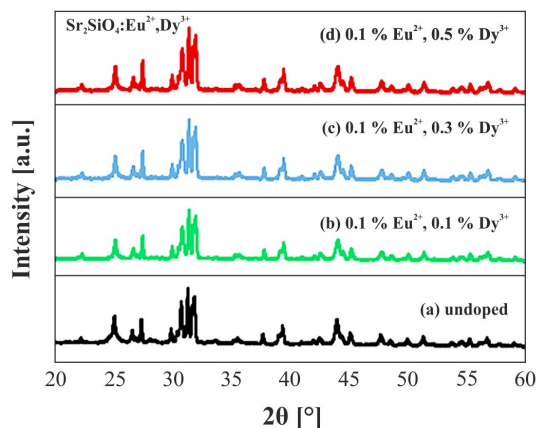


Fig. 2. XRD patterns of $\text{Sr}_2\text{SiO}_4:\text{Eu}^{2+}$ phosphors with different Dy^{3+} molar concentration.

a metastable state to ground state is forbidden [27]. The metastable state represents a shallow electron trap and electrons returning from it to the excited

state require energy. This energy can be supplied in the form of optical radiation or as heat.

Fig. 4a shows TL glow curve of $\text{Sr}_2\text{SiO}_4:\text{Eu}^{2+}, \text{Dy}^{3+}$ phosphor for different concentrations of Dy^{3+} from the range of 0.1 mol% to 0.4 mol%, while Eu^{2+} (0.1 mol%) is fixed. The peak position for all doping concentrations is 340.36 K only for the sample with 0.2 mol% concentration the glow peak is observed at 359.56 K.

TL intensity increases with increasing the doping concentration of Dy^{3+} , maximum signal is found for 0.2 mol%. The reason is that the increased number of defects/traps at a particular temperature may give rise to higher transition and consequently higher TL intensity was found [28]. The TL peak intensity increases at 0.2 mol% of Dy^{3+} and beyond this doping concentration, the TL intensity decreases due to concentration quenching.

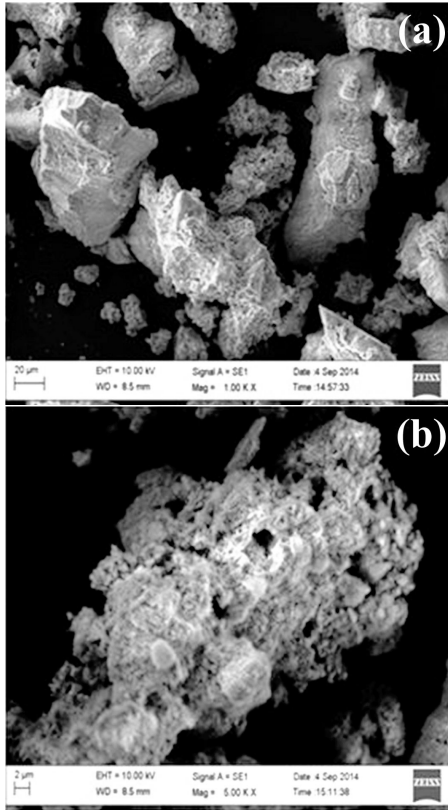


Fig. 3. SEM micrographs of $\text{Sr}_2\text{SiO}_4:\text{Eu}^{2+}, \text{Dy}^{3+}$ phosphor at different magnifications.

The decrease in the TL output when the dopant element is present in larger concentration is caused by the increased number of charge carriers being trapped upon irradiation. On being thermally stimulated, these traps release the charge carriers that finally recombine at the recombination centres and thus give rise to diverse glow peaks with increased height [29].

Using the Chen peak shape method [30] for determining the order of kinetics of TL glow curves, the kinetic order can be related to the geometrical factor μ_g by the relation:

$$\mu_g = \frac{T_2 - T_m}{T_2 - T_1} \quad (4)$$

where T_1 and T_2 ($T_1 < T_2$) are the temperatures at half maximum intensity and T_m is temperature of maximum intensity; $\delta = T_2 - T_m$, $\tau = T_m - T_1$ and $\omega = T_2 - T_1$, while E_δ , E_τ and E_ω are the corresponding activation energies. The shape factor

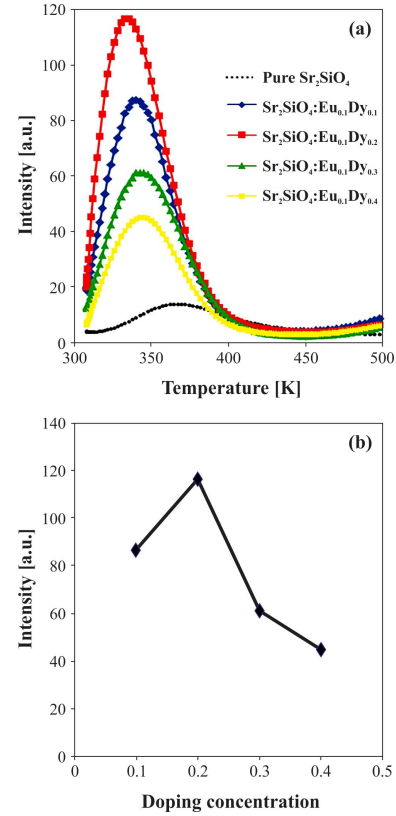


Fig. 4. (a) TL glow curves for $\text{Sr}_2\text{SiO}_4:\text{Eu}^{2+}$ with $\text{Eu}^{2+}(0.1)$, $\text{Dy}^{3+}(0.1 \text{ to } 0.4)$ for 20 min UV exposure with a heating rate 5 K/s; (b) variation of TL peak intensity with increasing Dy doping concentration.

($\mu_g = \delta/\omega$) is introduced to differentiate between first and second order TL glow peaks. $\mu_g = 0.39$ to 0.42 for the first order kinetics $\mu_g = 0.49$ to 0.52 for the second order kinetics and $\mu_g = 0.43$ to 0.48 for the mixed order of kinetics.

According to the relation, $\text{Sr}_2\text{SiO}_4:\text{Eu}^{2+}$ phosphor with different concentrations of co-doped (Dy^{3+}) shows the general order of kinetics and the activation energy is given by:

$$E_\alpha = C_\alpha \left(\frac{kT_m^2}{\alpha} \right) - b_\alpha(2kT_m) \quad (5)$$

The frequency factor was calculated by:

$$\frac{\beta E}{kT_m^2} = s \left[1 + (b-1) \frac{2kT_m}{E} \right] \exp(E/kT_m) \quad (6)$$

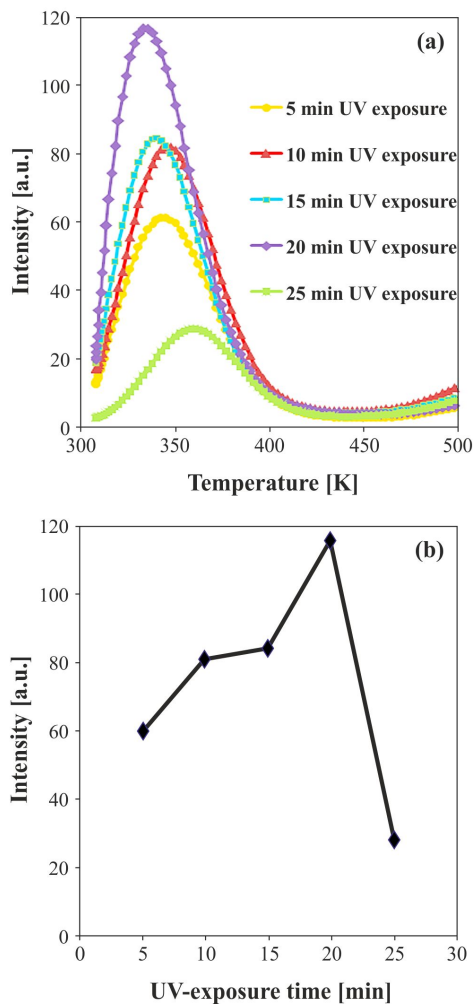


Fig. 5. (a) TL glow curves of $\text{Sr}_2\text{SiO}_4:\text{Eu}^{2+}(0.1)$, $\text{Dy}^{3+}(0.2)$ for different UV exposure times at a heating rate of 5 K/s; (b) variation of TL peak intensity with increasing UV exposure time.

The TL glow curves shown in Fig. 4a were recorded for a fixed UV exposure time, 20 min, and heating rate of 5 K/s. The values of different parameters calculated from the glow curves are presented in Table 2. The value of trap depth, which resembles the activation energy, has been calculated to lie between 0.50 eV to 0.61 eV. It is worth reporting that the shape factor μ_g , which ranges from 0.51 to 0.63, shows the second order kinetics that supports the probability of re-trapping of released charge carriers before recombination.

TL glow curves for the optimized concentration $\text{Sr}_2\text{SiO}_4:\text{Eu}^{2+}(0.1)$, $\text{Dy}^{3+}(0.2)$ at different UV

exposure times shown in Fig. 5a. We chose the doping concentration $\text{Eu}_{(0.1)}$ and $\text{Dy}_{(0.2)}$ because it gave the maximum TL intensity (Fig. 4). In Fig. 5a we can observe that TL intensity increases with increasing UV irradiation time. Further, there is no appreciable shift in the glow peak position toward higher temperature for higher irradiation doses. The thermoluminescence signal increases up to 20 minutes of UV exposure (Fig. 5b), then it starts to decrease. It is predicted that with the increasing UV exposure, the greater number of charge carriers are released which increases the trap density and results in an increase of thermoluminescence signals, but after 20 minutes of UV exposure, thermal quenching occurs and trap density starts to decline, which results in decreased TL intensity. The values of trap depth (E) with increasing UV exposure time as shown in Table 3.

3.5. Decay process

Decay of phosphors showing long-lived afterglow involves a rapid decay and a slow decay corresponding to the afterglow phosphorescence [31–33]. Fig. 6 shows the TL decay curve of $\text{Sr}_2\text{SiO}_4:\text{Eu}^{2+}(0.1)$, $\text{Dy}^{3+}(0.2)$ phosphor, indicating increased delay time, decreased intensity of the glow peak and the position of glow peak shifted toward higher temperatures because of retrapping of charge carriers (i.e. kinetic order > 1). The released carriers are retrapped before they recombine, giving rise to a delay in the luminescence emission and a spreading of the emission over a wider temperatures range [34].

Fig. 7 shows the decay curve of $\text{Sr}_2\text{SiO}_4:\text{Eu}^{2+}$, Dy^{3+} phosphor. The decay curve displaying TL intensity against time was plotted using the single exponential equation:

$$I = I_0 \exp \left[-\frac{t}{\tau} \right] \quad (7)$$

Here, the decay constant is τ and I_0 is a constant.

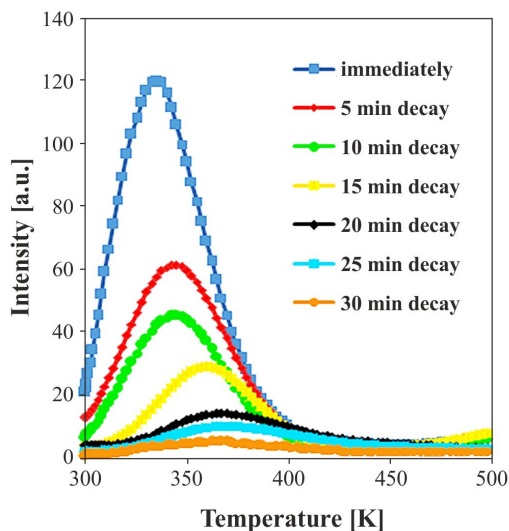
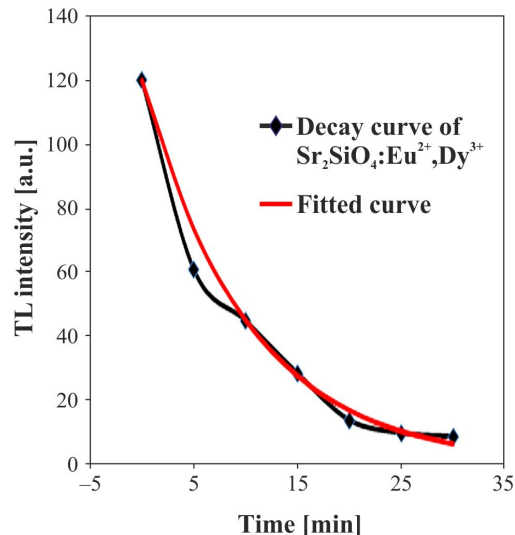
The decay constant was found to be 10.23 min. Table 4 shows the calculated kinetic parameters such as δ , ω , τ , μ_g (shape factor) and activation energy or trap depth (E) of $\text{Sr}_2\text{SiO}_4:\text{Eu}^{2+}$, Dy^{3+} phosphor which shows that trap depth increases with

Table 2. Kinetic parameters of $\text{Sr}_2\text{SiO}_4:\text{Eu}^{2+}(0.1), \text{Dy}^{3+}(0.1 \text{ to } 0.4)$ for 20 min UV exposure time.

Heating rate [K/s]	T_1 [K]	T_m [K]	T_2 [K]	τ	δ	$\mu_g = \delta/\omega$	Activation energy (trap depth) [eV]	Frequency factor
5	315.1	340.36	367	25.26	26.64	0.51	0.61	2.98×10^8
5	314	339.56	369	25.56	29.44	0.53	0.60	2.77×10^8
5	313	340.36	376.1	27.36	35.74	0.56	0.58	9.97×10^7
5	319.93	340.36	375.56	20.43	35.2	0.63	0.50	6.69×10^6

Table 3. Kinetic parameters of $\text{Sr}_2\text{SiO}_4:\text{Eu}^{2+}(0.1), \text{Dy}^{3+}(0.2)$ for different UV exposure times at a heating rate of 5 K/s.

UV exposure time [min]	T_1 [K]	T_m [K]	T_2 [K]	τ	δ	ω	$\mu_g = \delta/\omega$	Activation energy (trap depth) [eV]
5	312.36	342.81	373.61	30.45	30.8	61.25	0.50	0.50
10	317.96	342.23	371.19	24.4	28.83	53.23	0.54	0.65
15	316.43	340.36	370.1	24.36	29.74	54.1	0.55	0.65
20	313.2	335.56	358	22.36	22.44	44.8	0.50	0.66
25	331.13	360.39	388.48	29.26	28.09	57.35	0.49	0.57

Fig. 6. TL glow curves of $\text{Sr}_2\text{SiO}_4:\text{Eu}^{2+}(0.1), \text{Dy}^{3+}(0.2)$ for different decay times.Fig. 7. TL decay curve of $\text{Sr}_2\text{SiO}_4:\text{Eu}^{2+}(0.1), \text{Dy}^{3+}(0.2)$.

increasing delay time till the delay of 15 minutes. After that, it changes randomly which indicates that the traps became deeper till the delay of 15 min, and then they changed randomly. The value of the trap depth indicates that the phosphor has characteristics of a good and long-lasting material [35].

3.6. Photoluminescence studies

The photoluminescence spectra of $\text{Sr}_2\text{SiO}_4:\text{Eu}^{2+}(0.1), \text{Dy}^{3+}(0.2)$ are shown in Fig. 8a and Fig. 8b. The maximum TL intensity was found for $\text{Eu}^{2+}(0.1)$ and $\text{Dy}^{3+}(0.2)$ doping

Table 4. Calculated kinetic parameters of TL glow curves plotted after different decay times.

Decay time [min]	T ₁ [K]	T _m [K]	T ₂ [K]	τ	δ	ω	μ _g = δ/ω	Activation energy(trap depth) [eV]
Immediately	308.5	336.07	362.15	27.57	26.43	54	0.49	0.52
5	315.93	344.95	374.3	29.02	29.35	58.37	0.50	0.53
10	315.93	342.47	376.75	27.54	34.28	61.82	0.55	0.58
15	331.6	359.72	388.14	28.12	28.42	56.54	0.50	0.60
20	337	369.42	401	32.42	31.58	64	0.49	0.53
25	338.5	371.86	421	33.36	49.14	82.5	0.59	0.56
30	331.7	374.3	416.3	42.6	42	84.6	0.49	0.41

concentration so we chose this doping concentration for PL measurement. Fig. 8a shows the excitation spectrum, in the spectral region from 200 nm to 400 nm. It exhibits only one broad peak in the UV region centered at 245 nm. After UV excitation, the phosphor emits visible lights at a wavelength of 485 nm (blue), where a small peak is observed and at 560 nm (yellow) where a broad peak is seen (Fig. 8b). The broad absorption and emission spectra can be ascribed to the Eu²⁺ transition from 4f⁷ state to 4f⁷5d excited state [36]. Here, the luminescence centers correspond to Eu²⁺ ions, and any additional emission peak relating to Dy³⁺ ions in Sr₂SiO₄:Eu²⁺, Dy³⁺ phosphor is not observed. As expected, Dy³⁺ co-doped phosphor shows significant long-lasting afterglow properties [37].

The decay curve of Sr₂SiO₄: 0.1 mol % Eu²⁺, 0.2 mol% Dy³⁺ phosphor shown in Fig. 9 at the excitation wavelength of 245 nm generates emission of the wavelength of 560 nm for 120 s. A rapid intensity decrease at the initial stage is observed, then it slows down and finally a stable emission is achieved, followed by a slow decay process of long-lasting phosphorescence. Sr₂SiO₄:Eu²⁺, Dy³⁺ phosphors show the persistent luminescence because Dy³⁺ ions play an important role in the afterglow process. The Dy³⁺ ions act as deep hole trap levels, which are located between the ground and excited states of Eu²⁺. After excitation by UV light, ground states of Eu²⁺ excitation occurs as a result of electron and hole pairs generation from the ground state 4f to excited 4f 5d state. Some free

holes transported into the conduction band are captured by the Dy³⁺ traps. According to Jia et al. [38] Dy³⁺ transfers the electron to the excited Eu²⁺; the states as Dy⁴⁺ and Eu²⁺ are converted into Eu⁺. When UV excitation ends, the reversed route and the recombination of the hole and electron occurs to give bright and long-lasting phosphor [39].

4. Conclusions

In this work, Sr₂SiO₄:Eu²⁺, Dy³⁺ phosphor was prepared by combustion method which appears to be a very feasible method for production of this material. The band gaps of 5.52 eV and 5.4 eV for Sr₂SiO₄ and Sr₂SiO₄:Eu²⁺, Dy³⁺, respectively have been determined from the absorption spectra. Narrowing the band gap of 0.12 eV for Sr₂SiO₄:Eu²⁺, Dy³⁺ compared to pure Sr₂SiO₄ material shows the presence of impurity ions in the host material. XRD studies confirmed the formation of a single phase compound and the average crystallite size of Sr₂SiO₄:Eu²⁺, Dy³⁺ phosphor was found as 12.77 nm. SEM studies have shown that the particles are nonuniformly distributed in the material and form aggregates. TL glow curve of Sr₂SiO₄:Eu²⁺, Dy³⁺ phosphors rose with increasing the doping concentration of Dy³⁺, maximum signal occurred for 0.2 mol% Dy³⁺ and then the TL intensity decreased due to concentration quenching. TL intensity of the glow curve increased with increasing UV exposure time up to 20 min, after that it started to decrease. In thermoluminescence study, all peaks showed

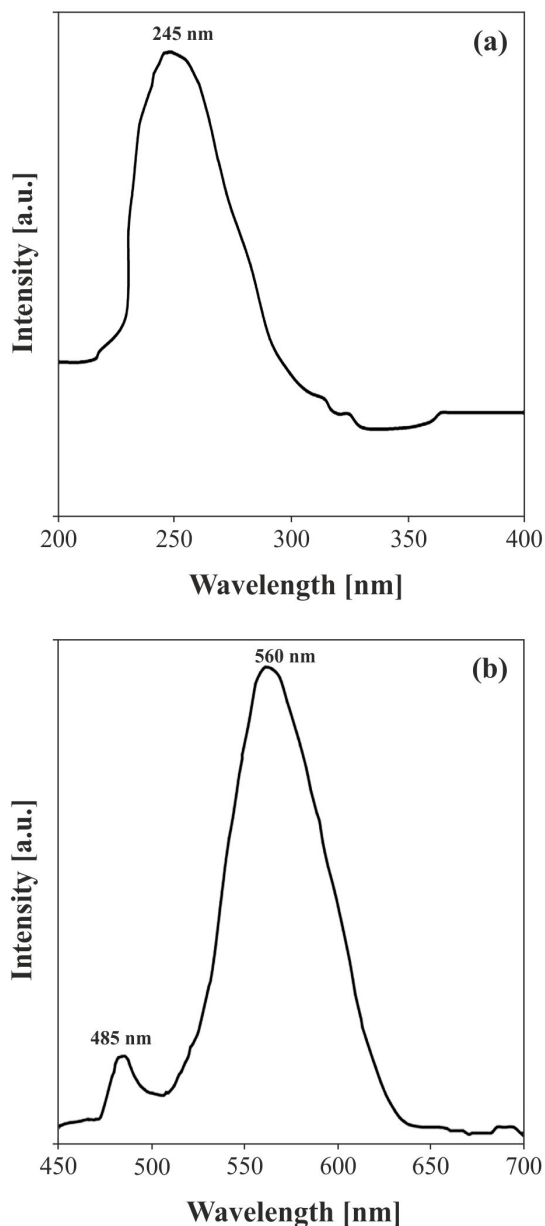


Fig. 8. (a) excitation spectra and (b) emission spectra of $\text{Sr}_2\text{SiO}_4:\text{Eu}^{2+}$ (0.1), Dy^{3+} (0.2) phosphor.

second-order kinetics which means that more than one luminescent center is present in the phosphor. PL spectra of $\text{Sr}_2\text{SiO}_4:\text{Eu}^{2+}$ (0.1), Dy^{3+} (0.2) phosphor exhibited strong emission peak 560 nm (yellow) and a weak 485 nm (blue) emission, when the phosphor was excited by 245 nm under UV region. The PL exponential decay curve showed that the phosphor has good luminescence properties.

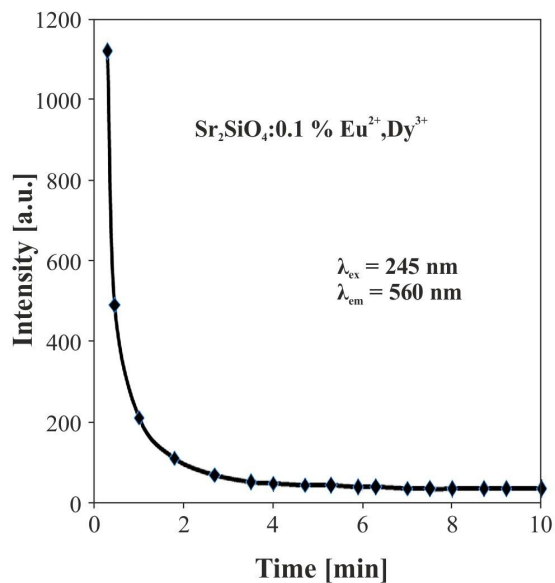


Fig. 9. Persistent luminescence of $\text{Sr}_2\text{SiO}_4:\text{Eu}^{2+}$ (0.1), Dy^{3+} (0.2) phosphor.

Acknowledgements

We gratefully acknowledge the kind support of the management of Shri Shankaracharya Group of Institutions (SSTC). The authors also thank the Department of Metallurgical Engineering, NIT Raipur, for help in the XRD and scanning electron microscopy (SEM) analysis of samples.

References

- [1] AYVACIKLI M., EGE A., YERCI S., CAN N., *J. Lumin.*, 131 (2011), 2432.
- [2] MATSUZAWA T., AOKI Y., TAKEUCHI N., MURAYAMA Y., *J. Electrochem. Soc.*, 143 (1996), 2670.
- [3] CATTI M., GAZZONI G., IVALDI G., ZANINI G., *Acta Crystallogr. C*, 39 (1983), 29.
- [4] HYDE B.G., SELLAR J.R., STENBERG L., *Acta Crystallogr. B*, 42 (1986), 423.
- [5] STENBERG L., HYDE B.G., *Acta Crystallogr. B*, 42 (1986), 417.
- [6] WU Z.C., SHI J.X., GONG M.L., WANG J., SU Q., *Mater. Chem. Phys.*, 103 (2007), 415.
- [7] BRICHE S., ZAMBON D., BOYER D., CHADEYRON G., MAHIOUET R., *Opt. Mater.*, 28 (2006), 615.
- [8] WU C., WANG Y., JIE W., *J. Alloy. Compd.*, 436 (2007), 383.
- [9] YU L.X., LI D.C., YUE M.X., YAO J., LU S.Z., *Chem. Phys.*, 326 (2006), 478.
- [10] YIN S.Y., CHEN D.H., TANG W.J., *J. Alloy. Compd.*, 441 (2007), 327.
- [11] XU L., WEI B., ZHANG Z., LU Z., GAO H., ZHANG Y., *IOP Publishing Ltd. Nanotech.*, 17 (2006), 4327.

- [12] ZHANG J., NING J., LIU X., PAN Y., HUANG L., *Mater. Res. Bull.*, 38 (2003), 1249.
- [13] BANG J., ABOUDI M., ABRAMS B., HOLLOWAY P.H., *J. Lumin.*, 106 (2004), 177.
- [14] MCKEEVER S.W.S., *Thermoluminescence of Solids*, Cambridge Solid State Science Series, Cambridge, 1985.
- [15] NAMBI K.S.V., *Thermoluminescence its understanding and applications*, Instituto de Energia Atomica – Sao Paulo, Brazil, 1977.
- [16] CHAKRADHAR R.P.S., NAGABHUSHANA B.M., CHANDRAPPA G.T., RAMESH K.P., RAO J.L., *J. Chem. Phys.*, 121 (2004), 10250.
- [17] HARANATH D., CHANDER H., SHARMA P., SINGH S., *Appl. Phys. Lett.*, 89 (2006), 173118.
- [18] TAUC J., MENTH A., *J. Non-Cryst. Solids*, 8 – 10 (1972), 569.
- [19] TAUC J., *Mater. Res. Bull.*, 3 (1968), 37.
- [20] TAUC J., GRIGOROVICI R., VANCU A., *Physica Status Solidi B*, 15 (1966), 627.
- [21] BUCHHOLZ D.B., LIU J., MARKS T.J., ZHANG M., CHANG R.P.H., *ACS Appl. Mater. Inter.*, 1(2009), 2147.
- [22] VIJAYALAKSHMI S., VENKATARAJ S., SUBRAMANIAN M., JAYAVEL R., *J. Phys. D*, 41 (2008), 035505.
- [23] MAYANDI J., MARIKKANNAN M., RAGAVENDRAN V., JAYABAL P., *J. Nanosci. Nanotechnol.*, 2 (2014), 707.
- [24] FEITOSA A.V., MIRANDA M.A.R., SASAKI J.M., ARUJO-SILVA M.A., *Braz. J. Phys.*, 34 (2004), 656.
- [25] UBALE A.U., SANGAWAR V.S., KULKARNI D.K., *B. Mater. Sci.*, 30 (2007), 147.
- [26] SUNITHA D.V., MANJUNATHA C., SHILPA C.J., NAGABHUSHANA H., SHARMA S.C., NAGABHUSHANA B.M., *Spectrochim. Acta A*, 99 (2012), 279.
- [27] MCKEEVER S.W.S., *Thermoluminescence of Solids*, Cambridge University Press, Cambridge, 1985.
- [28] XINGDONG L., MINJUAN Z., RENQIN W., *J. Wuhan Univ. Tech.-Mater. Sci.*, 23 (2008), 652.
- [29] CHEN R., LAWLESS J.L., PAGONIS V., *Radiat. Meas.*, 46 (2011), 1380.
- [30] CHEN R., *J. Electrochem. Soc.*, 116 (1969), 1254.
- [31] KUBO H., AIZAWA H., KATSUMATA T., KOMURO S., MORIKAWA T., *J. Cryst. Growth*, 275 (2005), 1767.
- [32] SHARMA S.K., PITALE S.S., MALIK M.M., QURESHI M.S., DUBEY R.N., *J. Alloy. Compd.*, 482 (2009), 468.
- [33] WU H., HU Y., ZENG B., MOU Z., DENG L., *J. Phys. Chem. Solids*, 72 (2011), 1284.
- [34] WU H., HU Y., WANG X., *Radiat. Meas.*, 46 (2011), 591.
- [35] MASHANGVA M., SINGH M.N., SINGH B., *Indian J. Pure Appl. Phys.*, 49 (2011), 583.
- [36] AKIYAMA M., XU C.N., NONAKA K., WATANABE T., *Appl. Phys. Lett.*, 73 (1998), 3046.
- [37] MATSUZAWA T., AOKI Y., TAKEUCHI N., MURAYAMA Y., *J. Electrochem. Soc.*, 143 (1996), 2670.
- [38] JIA W., YUAN H., LU L., LIU H., YEN W.M., *J. Lumin.*, 76 (1998), 424.
- [39] YAMAMOTO H., MATSUZAWA T., *J. Lumin.*, 72 (1997), 287.

Received 2017-03-16

Accepted 2017-02-19